Numerical study of the gas flow velocity space in convection reflow oven

Balázs Illés and István Bakó
Budapest University of Technology and Economics
Department of Electronics Technology
Egry József. u. 18, H-1111 Budapest, Hungary
billes@ett.bme.hu

Abstract: In this paper, numerical study of the gas flow velocity space is presented in a convection type reflow oven. Convection reflow ovens usually apply the nozzle-matrix heater system which generates numerous gas streams perpendicularly to surface of the soldered assembly. The ovens are divided into zones; every zone contains an upper and a lower nozzle-matrix. The temperature can be independently controlled in each zone; however the velocity of the influent streams is usually fixed. The gas flow velocity space is one of the most important parameter of the local heat transfer coefficient in the oven. The gas flow space cannot be examined by classical experimental methods due to the extreme circumstances in the reflow oven. Therefore the effect of the soldered assembly, the different component sizes, the position of the conveyor belt and the vent hood between the zones on the gas flow velocity space was studied by CFD simulations. These results can be useful during the overview of the actual assembly design and manufacturing rules.

Keywords: convection reflow oven, CFD, gas flow velocity, reflow soldering.

Nomenclature

		κ	turbulent kinetic energy, [m^2/s^2]
x,y,z	coordinates, [m]	ε	turbulent dissipation rate, [m^2/s^3]
u	velocity, [m/s]	δ_{i3}	Kronecker tensor
p	pressure, [Pa]	R	gas constant
ρ	density, [kg/m^3]	C	constant of k-ε model
t	time, [s]	σ	Prandtl number
T	temperature, [K]	g	gravity force
μ	dynamic viscosity, [m^2/s]		
μ_t	turbulent dynam. eddy visc., [m^2/s]	*Superscript*	
α	thermal diffusivity, [m^2/s]	$\bar{}$	Average value

1. Introduction

Reflow soldering is the most widespread soldering technology used in the electronics industry for surface mounted technology (SMT). This process is applied when surface mount devices (SMDs) are attached to printed wiring boards (PWBs). The preparatory steps of the process are the printing of solder paste to the contact surfaces (pads) of the PWB, and the component placement onto the deposited solder paste. The reflow process heats the entire assembly to a temperature beyond the melting point of the solder alloy which wets the contact surfaces and forms the joints [1, 2].

Usually the heating of the assembly is achieved by a convection reflow oven which mainly applies the nozzle-matrix heater system. The nozzle-matrix generates numerous gas streams perpendicularly to surface of the soldered assembly. The ovens are divided into zones (6-12 zone is usual); every zone contains an upper and a lower nozzle-matrix [3]. The temperature can be independently controlled in each zone; however the velocity of the inflowing streams is usually fixed. Due to the nature of convection heating the temperature distribution in the zones is near homogeneous [4, 5]. Therefore the heating performance of convection reflow ovens mainly depends on the heat transfer coefficient distribution in the process volume of the oven. The main influential factor on the heat transfer coefficient is the velocity and the character (laminar or turbulent) of the gas flow space [6]. The homogeneity and the efficiency of the heat transport have strong influence on the quality of the solder joints [1].

The temperature can reach 250 ºC in some zones and the process volume of the oven can be considered as a tube with 8-10 m length and only 6-9 cm height. These extreme circumstances exclude most of the typical flow measurement methods. Therefore the most effective tool of the reflow oven researches was always the approach of simulation. The first heating capability examinations of reflow ovens were started with simple simulations (using only 2 dimensions with low resolution) [7, 8]. Some newer thermal models of the reflow process still an average heat transfer coefficient [2, 9]. Later it was proven that the changes of the gas flow parameters, the inhomogeneity of the gas circulation system and the different contamination level of the nozzles can considerably modify the heat transfer coefficients distribution in the oven [5, 10].

Only a limited number of publications deal with the study of multi-zone constructed convection reflow ovens for mass production. Some authors concentrate only a specific

part of the process, e.g. for the preheating phase [4, 11] or for the cooling stage of the assembly [12]. A method for optimizing the heating capability of heater gas streams in convection reflow ovens was carried out by the geometry and dimension modifications of the nozzles [13]. Inoue [14] has approximated the heat transfer coefficient of the heater gas streams from the nozzle-matrix blower system with the systematic series of experiments. The direction characteristics of the heat transfer coefficient were also studied by temperature measurements [10, 15]. Application of statistical methods (e.g. Taguchi) [16] or soft computing (e.g. genetic algorithms) [17] also can be found for optimizing the reflow ovens capabilities.

Some partial effects of the assembly with flat components on the gas flow velocity space was examined by Lau [4], however there is a need for deeper analyses about the effect of different component sizes, the position of the conveyor belt and the vent hood between the zones which results can be useful during the overview of the actual assembly design and manufacturing rules.

2. METHODOLOGY

2.1 The Investigated Reflow Oven

The investigated reflow oven contains seven heater zones (the first five are pre-heater zones and then the next two are peak zones) and one cooler zone (the last zone). The schematic cross-sectional view of the heater system in the investigated convection reflow oven can be seen in Fig. 1.

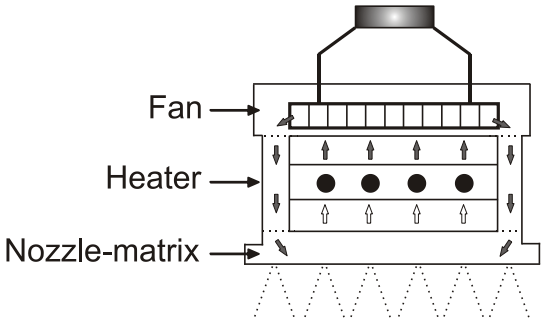

Fig. 1. Cross-section view of the heater system in the investigated reflow oven.

The main parts of the heater zones are the following: electrical heater modules which heat the gas, a fan which moves the gas, a nozzle-matrix which distributes the moving gas above the assembly and generates the heater gas streams. The construction of the

heater and the cooling system is the same but the cooling system does not contain electrical heaters.

The nozzle-matrixes are 560 mm wide and 415 mm long (towards the moving direction of the assembly). They contain 42 parallel nozzle-lines with 8 nozzles in each line which are also parallel with the moving direction of the PWB. The distance of the nozzles in the lines is 50 mm and the distance of the nozzle-lines is 26 mm. The neighbouring nozzle-lines are shifted a half raster, so the nozzles are located in the vertices of near equal triangles. The nozzle diameter is 5.5 mm. The distance between the nozzle-matrix and the PWB is usually 20–40 mm (this parameter was varied during the simulations). The height of the zones is 60 mm.

The inner arrangement of the investigated reflow oven can be seen in Fig. 2. During the soldering process, the assembled PWB is drifted on a conveyor line between the upper and lower nozzle-matrices.

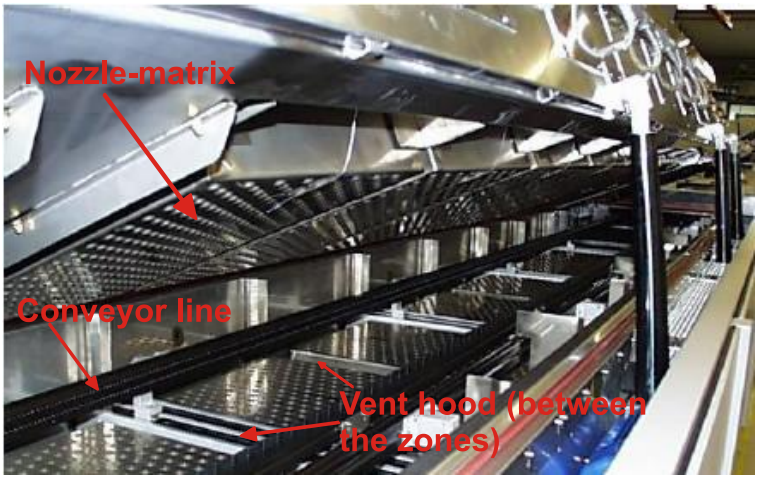

Fig. 2. Inner arrangement of the investigated reflow oven (during the operation the oven is closed).

A typical 175 mm width was applied for the conveyor line. The investigated reflow oven was designed for double conveyer line; however a lot of users apply them with only one conveyor. In this case the position of the conveyor line is asymmetric, the distance from the right and left wall of the oven is 175 and 385 mm, respectively. This conveyor arrangement can effect on the gas flow space therefore this case was studied.

2.1 Modelling Approach

The gas flow velocity model in the zones of the oven based on the following criteria: the vertical gas streams from the nozzle-matrix are laminar and join into a continuous radial flow layer above the board. (The model of an inlet vertical gas stream can be seen in [5, 10]). The radial flow layer has dominant flow directions towards entrance and exit of the zones, however it becomes turbulent due the obstruction points in the zone (walls, the assembly, etc.). From the turbulent CFD methods the Reynolds Averaged Navier-Stokes (RANS) was applied with the standard κ-ε model in order to calculate the Reynolds stresses coming from the averaging [18]. The RANS equations compute the averaged motion and model the effect of fluctuations. The κ-ε model performs well in cases of non-large adverse pressure gradients [19]. It belongs to the "two equation models" that means it includes two extra transport equations to describe the turbulent properties of the flow. This allows accounting for "history" effects of convection and diffusion of turbulent energy.

The air flow in the zones is governed by the Navier–Stokes equation:

$$\frac{\partial}{\partial t}(\rho u_i) + \frac{\partial}{\partial x_j}(\rho u_j u_i) = \frac{\partial p}{\partial x_i} + \mu \frac{\partial}{\partial x_j}\left(\frac{\partial u_i}{\partial x_j} + \frac{\partial u_j}{\partial x_i}\right) - \rho g \delta_{i3} \tag{1}$$

where u is the gas flow velocity, ρ is the density, p is the pressure, μ is the dynamic viscosity, g is the gravity force and δ_{i3} is the Kronecker tensor. During the description of the modeling approach the coordinates is denoted with index notation. Using the averaging form to the Navier-Stokes equations results in [20]:

$$\frac{\partial}{\partial t}\left(\overline{\rho}\overline{u_i}\right) + \frac{\partial}{\partial x_j}\left(\overline{\rho}\overline{u_j}\overline{u_i}\right) = \frac{\partial \overline{p}}{\partial x_i} + \frac{\partial}{\partial x_j}\left[\left(\mu + \mu_t\right)\left(\frac{\partial \overline{u}_i}{\partial x_j} + \frac{\partial \overline{u}_j}{\partial x_i}\right)\right] - \overline{\rho} g \delta_{i3} \tag{2}$$

where the bars marks the time averages and the turbulent stresses is described through the turbulent dynamic eddy viscosity μ_t. According the κ-ε model, if the turbulence is isotropic the turbulent kinetic energy (κ) and the turbulent dissipation rate (ε) – to distinguish between large and small eddies – determines the turbulent dynamic eddy viscosity:

$$\mu_t = \overline{\rho} C_\mu \frac{\kappa^2}{\varepsilon} \tag{3}$$

where C_μ is a constant with 0.09 value. Finally the κ-ε model for the turbulent kinetic energy and dissipation is the following [20]:

$$\frac{\partial}{\partial t}\left(\overline{\rho}\overline{\kappa}\right)+\frac{\partial}{\partial x_j}\left(\overline{\rho}\overline{u}_i\overline{\kappa}\right)=\frac{\partial}{\partial x_i}\left[\left(\frac{\mu+\mu_t}{\sigma_\kappa}\right)\frac{\partial\kappa}{\partial x_j}\right]+G-\overline{\rho}\varepsilon \tag{4}$$

$$\frac{\partial}{\partial t}\left(\overline{\rho}\overline{\varepsilon}\right)+\frac{\partial}{\partial x_j}\left(\overline{\rho}\overline{u}_i\varepsilon\right)=\frac{\partial}{\partial x_i}\left[\left(\frac{\mu+\mu_t}{\sigma_\varepsilon}\right)\frac{\partial\varepsilon}{\partial x_j}\right]+GC_1\frac{\varepsilon}{\kappa}-C_2\overline{\rho}\frac{\varepsilon^2}{\kappa} \tag{5}$$

where $\sigma_\kappa = 1$ and $\sigma_\varepsilon = 1.22$ are the equivalent Prandtl numbers for the turbulent diffusion of kinetic energy and dissipation. G is the rate of production of turbulent kinetic energy by the action of the mean-flow velocity gradient tensor against the turbulent stresses:

$$G=\left(\mu+\mu_t\right)\frac{\partial\overline{u}_i}{x_j}\left(\frac{\partial\overline{u}_i}{\partial x_j}+\frac{\partial\overline{u}_j}{\partial x_i}\right) \tag{6}$$

The applied constants were the followings: $C_1 = 1.44$; $C_2 = 1.92$. Previously defined constants (C_μ, C_1 and C_2) have been determined from experiments with air and water for fundamental turbulent shear flows including homogeneous shear flows and decaying isotropic grid turbulence. They have been found to work well for a wide range of wall-bounded and free shear flows with a wide range of different fluids [21].

The turbulent transport of energy is modeled in a similar way [20, 22]:

$$\frac{\partial}{\partial t}\left(\overline{\rho}\overline{T}\right)+\frac{\partial}{\partial x_j}\left(\overline{\rho}\overline{u}_i\overline{T}\right)=\frac{\partial}{\partial x_i}\left[\left(\alpha+\frac{\mu_t}{\sigma_T}\right)\frac{\partial\overline{T}}{\partial x_j}\right] \tag{7}$$

where T is temperature, α is thermal diffusivity and σ_T the turbulent thermal Prandtl number for the temperature. For the complete equation system, the continuity equation:

$$\frac{\partial\overline{\rho}}{\partial t}+\frac{\partial}{\partial x_i}\left(\overline{\rho}\overline{u}_i\right)=0, \tag{8}$$

and the ideal gas equation of state were also used for the calculation of the mean density:

$$\overline{\rho}=\frac{\overline{p}}{R\overline{T}} \tag{9}$$

where R is the gas constant.

3. MODELLING RESULTS

The model was solved by Finite Volume Method (FVM) and was constructed in Fluent modeling software. The model of one heater zone was created since every zone has the same parameters expect of the inlet gas temperature. Structured mesh was applied with 0.5 mm uniform mesh size. The following material parameters were used for the inflowing air: temperature 400 K, density 0.884 kg/m^3, dynamic viscosity 2.289E-5 kg/m.s and velocity 3.7 m/s^2 (given velocity value in the studied oven). The nozzles are velocity inlets with normal velocity direction. During the simulation the *x* direction points toward the moving direction of the soldered assembly, *y* direction points towards the walls of the zone and *z* direction points towards the height of the zone.

3.1 Initial Calculations

The initial calculations were done without soldered assembly in the zone. The results of the initial calculations can be seen in Fig. 3 along an *x*-*z* and an *y*-*z* cross-section of the zone, 10^{-6} convergence criterion was applied.

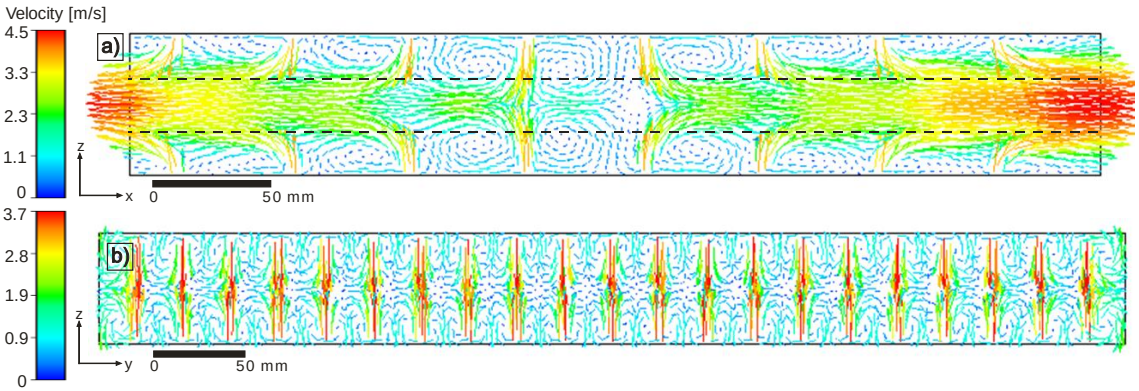

Fig. 3. Gas flow velocity space: a) *x*-*z* cross-section of the zone at the middle; b) *y*-*z* cross-section of the zone at the middle.

The results show that the gas streams forms two lateral flows which are laminar towards the in- and outlet of the zone as it was expected according to our previous measurements [5, 10]. The velocity of the lateral flows increasing towards the in- and

outlets of the zones and reaches significantly higher value (~4.5 m/s) then the velocity of the gas streams (3.7 m/s). Besides, the gas flow velocity is very low in the center region of the zone. This effect results in that the heat transfer coefficient changes highly towards the *x* direction of the zones (and also the oven). An effective heating area of the zones is also marked in Fig. 3a) what is around 20mm wide and located at the center of the zones along the *x* direction. Over and under the lateral flows the gas flow is turbulent with ~0.8 – 1.2 m/s velocities. The lateral flows are asymmetric a bit due to the asymmetric position of the nozzles along the *x* direction.

The results in the *x*-*y* cross-section show more homogeneous gas flow space then in the *x*-*z* cross-section. The gas can leave the zones only towards the *x* direction; therefore lateral flow effect is much lower here. This results in a near homogeneous heat transfer along the *y* direction of the zones which probably also compensate the inhomogeneity towards the *x* direction. The walls of the oven causes higher turbulence near the walls the velocity can reach 2 m/s, but this region is unused during the soldering.

The effect of the vent hood system between the zones was also investigated. The distance between the zones is 100 mm and the height of the vent hood is 85 mm upward and downward equally. According to the results the effect of the vent hood is negligible during the further calculations (Fig. 4).

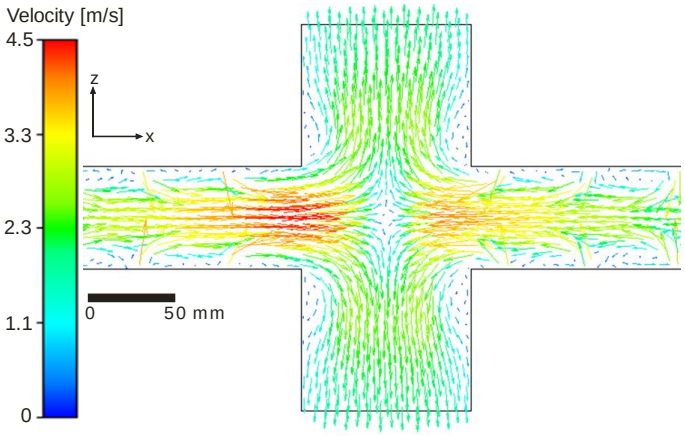

Fig. 4. Effect of the vent hood between the zones.

Finally a pure FR-4 board (with 175x175x1 mm dimensions) was positioned equally from the top and bottom of the zone along the *x* direction and from 175 mm of the left wall along the *y* direction (given distance in the studied oven) in order to study the effect of the board on the gas flow model. The results can be seen in Fig. 5. Along the *x*

direction the effect of the board was studied in several different positions (simulating the path of the board in the oven), Fig. 5 contains only one example.

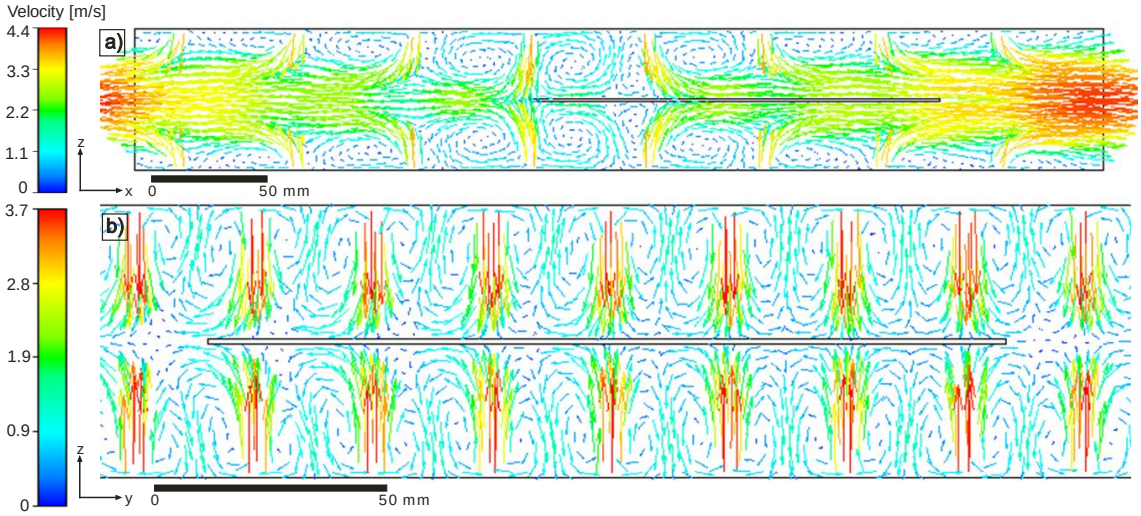

Fig. 5. Gas flow velocity space with a test board: a) *x*-*z* middle cross-section of the zone; b) a part of *y*-*z* middle cross-section of the zone.

It was found that the test board has only a minor effect on the gas flow space – the maximum velocities decreases a bit along the *x* direction – if it is positioned equally (30-30mm) from the top and bottom of the zone. The flow is near laminar next to the board. The calculations have also shown that the gas flow velocity model can be considered to be stationary, as it was expected according to the pervious works which have found only small temperature gradients in the zones [4, 5]. These small temperature gradients have only a minor effect on the gas flow space. In addition the initial calculations have also proved that the buoyancy flux can be neglected, since the calculations were also invariant for the effect of gravity due to the relatively high gas flow velocity. These facts decrease considerably the necessary calculation time.

3.2 Effect of different factors on the gas flow velocity space

In the first step the effect of the asymmetric board position along the *x* direction (moving direction of the board in the oven) was investigated. The board was lowered 10 mm towards the bottom of the oven. Similar arrangements are usually used in the electronics industry due to the different height of the oven and the supplying conveyor systems. The important part of results can be seen in Fig. 6. The asymmetric position of

the board considerably increases the lateral gas flow velocity (and also the heat transfer) over the board along the *x* direction. The change is negligible under the board. On the other hand, along the *y* direction the gas flow velocity increases under the board, however maximum velocity increase is not presented. Some side effects are visible at the corner of the board (Fig. 6b)). These opposite effects along the different directions can balance each other.

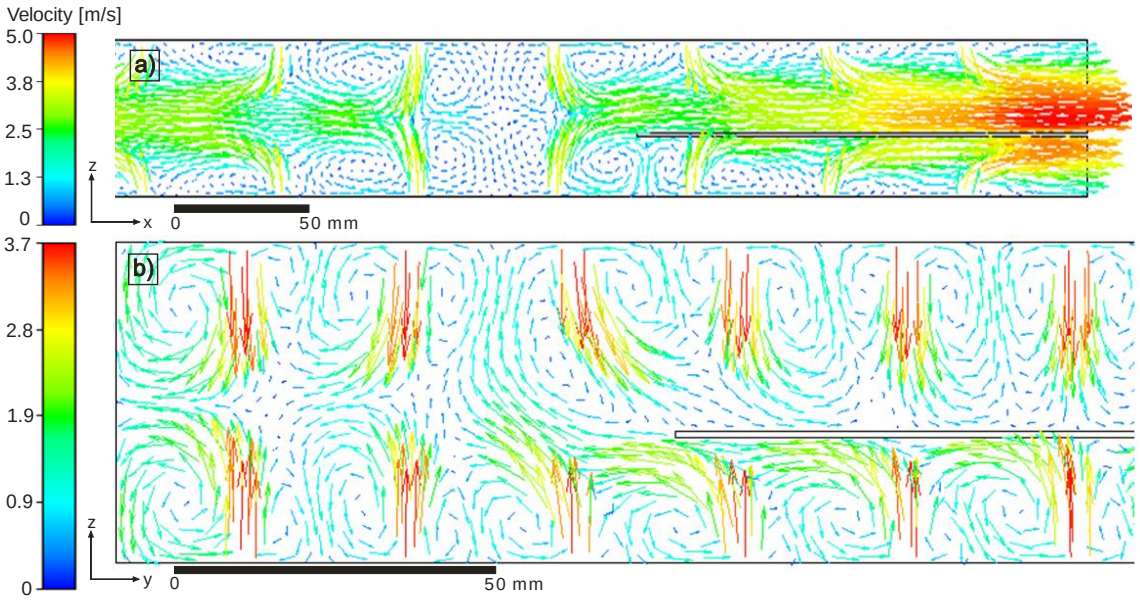

Fig. 6. Effect of the asymmetrical board position. a) a part of *x*-*z* middle cross-section of the zone; b) a part of *y*-*z* middle cross-section of the zone.

In the next step the effect of surface mounted components on the gas flow velocity space was investigated. Two different component types were studied: a columnar with 8x8x10 mm size (e.g. electrolyte capacitor or TO-2xx package) and a flat with 15x15x1.5 mm (e.g. BGA or QFP package). The results can be seen in Fig. 7. Along the *x* direction, the columnar component perturbs the lateral flow (Fig. 7a)-b)) which has to step over the component. This results in shadowed area first at the left side of the component (up to the middle of the zones) and then at the right side of the component (Fig. 7a)-b)) where the gas flow space is turbulent in each and the velocity is almost zero. According to the results the size of the shadowed area grows with the velocity of the lateral flow layer. In addition the flow velocity is always low at lower part of the component where the soldering is happened. Unfortunately this results in

inhomogeneous heating of the component which can cause the displacement big size components [23].

Along the *y* direction, the effect of the columnar component is not considerable on the gas flow space. If the component is located between two nozzles (Fig. 7c)) it draws the gas streams to them self what can help the heat transfer. According to these results, in the case of columnar components the heat transfer is more homogeneous and efficient along the *y* direction then along the *x*. This is also valid for the adjacent area of the columnar component; therefore the placement of small component next to a columnar one is not practical along the *x* direction. The effect of the flat component is negligible along both directions. The simulation results were invariant for the change of the component positions (up/down side of the board).

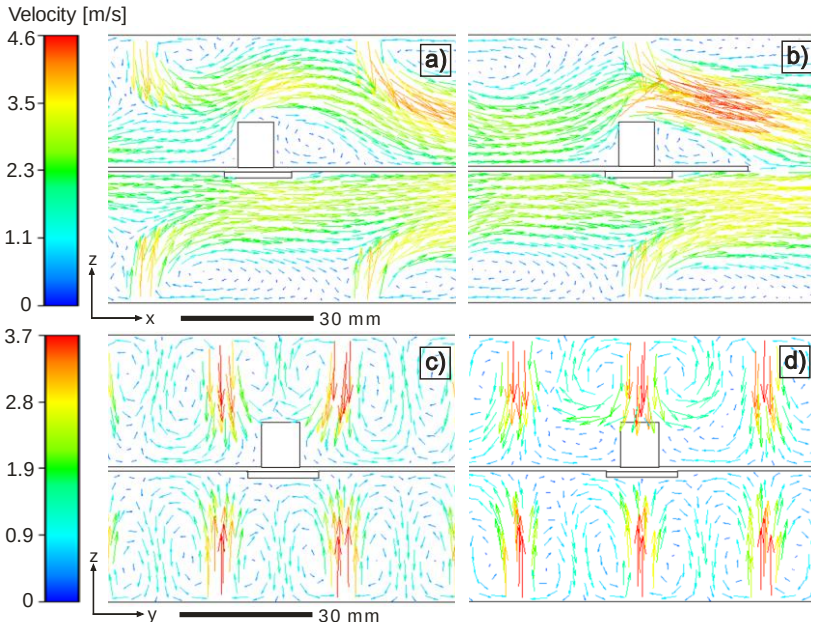

Fig. 7. Effect of the components. a) components between the nozzles, a part of *x*-*z* middle cross-section; b) components under a nozzle, a part of *x*-*z* middle cross-section; c) components between the nozzles, a part of *y*-*z* middle cross-section; d) components under a nozzle, a part of *y*-*z* middle cross-section.

The effect of neighboring columnar components was also studied on both sides of the board. The applied distances were 12.5, 25 and 50 mm (measured between the centers of the components) which means a quarter, a half and one nozzle distance along the *x* direction, respectively. If the distance is only a quarter nozzle distance the gas flow

velocity is almost zero between the component along both directions (Fig. 8a) and d)). At half nozzle distance the gas flow velocity reaches ~1 – 1.5 m/s between the components along both directions (Fig. 8b) and d)), depending on the actual position in the zone. In the case of one nozzle distance the effect of the neighbors are negligible (Fig 8c)), the results are the same as in the case of only one columnar component (Fig. 7). Therefore, it can be concluded that minimum distance between columnar components should be at least a half nozzle distance along the *x* direction of the applied oven. The simulation results were invariant for the change of the component positions (up/down side of the board).

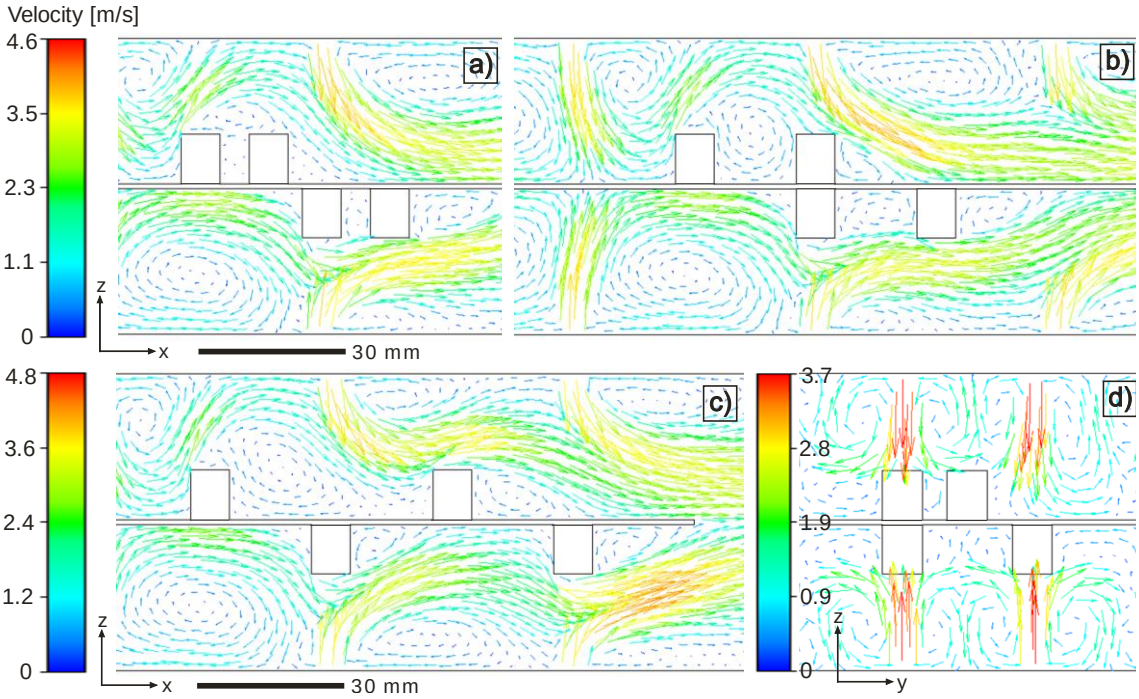

Fig. 8. Effect of neighboring columnar components. a) 12.5 mm distance, a part of *x*-*z* middle cross-section; b) 25 mm distance, a part of *x*-*z* middle cross-section; c) 50 mm distance, a part of *x*-*z* middle cross-section; d) 12.5 and 25 mm distance, a part of *y*-*z* middle cross-section.

3.3 Suggestions on assembly design

According to the obtained results, the following suggestions on the assembly design can be given:

1. Total thickness of the assembly should not be exceeded ~20mm, due to the size of the effective heating area (defined in Section 3.1). This parameter can vary a bit in the different ovens; therefore refinement is suggested by CFD modeling.
2. Different heat transfer coefficients can be achieved between the sides of the assembly by asymmetric board position along the moving direction of the board. This can be useful in the case of double sided reflow process where the heating gradient of the first reflowed side should be smaller.
3. Flow velocity is decreased at the lower edges of columnar components (where the solder joints are located) which results in decrease of the heat transfer coefficient at that regions. In addition the columnar components can shadow the small ones next to them. Therefore the application of components which are higher than ~5 mm is not suggested.
4. In the case of application of columnar components the minimum distance between them should be at least a half nozzle distance along the moving direction of the board in the oven.
5. According to the previously discussed points, the assembly design is more critical along the moving direction of the board in the oven than towards the walls of the oven.

5. Conclusions

CFD simulations of the gas flow velocity space in a convection reflow oven were conducted with κ-ε turbulent method. It was found that the gas streams forms two lateral flows which are laminar with increasing velocity towards the in- and outlet of the zone, while the gas flow velocity is very low in the center region of the zone. The *x*-*y* cross-section show more homogeneous gas flow space then the *x*-*z* cross-section. This results that the heat transfer coefficient changes highly towards the *x* direction and it is near homogeneous along the *y* direction of the zones. It has been proved that the effect of the vent hood system between the zones is negligible. It was found that the asymmetrical board position along the *x* direction considerably increases the lateral gas flow velocity over the board but under it the change is negligible. On the other hand, along the *y* direction this effect was found to give the opposite result.

The columnar components perturb the lateral flow along the *x* direction which results in temporarily shadowed areas at the lower corners of the component, while along the *y* direction this effect is not existed. According to these results, in the case of columnar components the heat transfer is more homogeneous and more efficient along the *y* direction then along the *x*. This can cause soldering failures of the columnar component and the adjacent small components. It was observed, that the shadowing effect of the neighboring columnar components is negligible over one nozzle distance between them. However, the minimum distance between columnar components should be at least a half nozzle distance along the *x* direction of the applied oven. These results can be useful during the overview of the actual assembly design and manufacturing rules.

6. Acknowledgement

This paper was supported by the János Bolyai Research Scholarship of the Hungarian Academy of Sciences.

References

[1] O. Krammer, I. Kobolák , L.M. Molnár, Method for selective solder paste application for BGA rework. Proceedings of 31st International Spring Seminar on Electronics Technology. Budapest, Hungary, 2008, pp. 432-436.

[2] D.C. Whalley, A simplified reflow soldering process model, Journal of Materials Processing Technology 150 (2004) 134–144.

[3] C.S. Lau, M.Z. Abdullah, F.C. Ani, Computational Fluid Dynamic and Thermal Analysis for BGA Assembly during Forced Convection Reflow Soldering Process, Soldering & Surface Mounting Technology 24/2 (2012) 77-91.

[4] C. S. Lau, M. Z. Abdullah, F. C. Ani, Three-Dimensional Thermal Investigations at Board Level in a Reflow Oven Using Thermal-Coupling Method, Soldering & Surface Mounting Technology 24/3 (2012) 167-182.

[5] B. Illés, Distribution of the heat transfer coefficient in convection reflow oven, Applied Thermal Engineering 30 (2010) 1523–1530.

[6] W. Kays, M. Crawford, B. Weigand, Convective Heat and Mass Transfer, 2004, 4th Ed., McGraw-Hill Professional.

[7] F. Sarvar, P.P. Conway, Effective modelling of the reflow soldering process: basis construction and operation of a process model, IEEE Transactions on Components, Packaging and Manufacturing Technology Part C: Manufacturing 21 (2) (1998) 126–133.

[8] C-H. Wu, K. Srihari, A.J. McLenaghan, A knowledge-based thermal profile identification advisor for surface mount PCB assembly, International Journal of Advanced Manufacturing Technology 11 (1996) 343–352.

[9] N.V. Steenberge, P. Limaye, G. Willems, B. Vandevelde, I. Schildermans, Analytical and finite element models of the thermal behavior for lead-free soldering processes in electronic assembly, Microelectronics Reliability 47 (2007) 215-222.

[10] B. Illés, G. Harsányi, Investigating direction characteristics of the heat transfer coefficient in forced convection reflow oven, Experimental Thermal and Fluid Science 33 (2009) 642–650.

[11] I. Belov, M. Lindgren, P. Leisner, F. Bergner, R. Bornoff, CFD Aided Reflow Oven Profiling for PCB Preheating in a Soldering Process, IEEE Proceedings of EuroSime Conference, London, England, 2007, pp. 1–8.

[12] C.-S. Lau, M. Z. Abdullah, F. C. Ani, Effect of Solder Joint Arrangements on BGA Lead-Free Reliability During Cooling Stage of Reflow Soldering Process, IEEE Transactions on Components, Packaging and Manufacturing Technology 2/12 (2012) 2098-2107.

[13] M. Yamane, N. Orita, K. Miyazaki, W. Zhou, Development of New Model Reflow Oven for Lead-Free Soldering, Furukawa Review 26 (2004) 31–36.

[14] M. Inoue, T. Koyanagawa, Thermal Simulation for Predicting Substrate Temperature during Reflow Soldering Process, IEEE Proceedings of 55th Electronic Components and Technology Conference, Lake Buena Vista, Florida, 2005, pp. 1021-1026.

[15] B. Illés, Measuring heat transfer coefficient in convection reflow ovens, Measurement 43 (2010) 1134–1141.

[16] C.S. Lau, M.Z. Abdullah, F.C. Ani, Optimization modeling of the cooling stage of reflow soldering process for ball grid array package using the gray-based Taguchi method, Microelectronics Reliability 52 (2012) 1143-1152.

[17] T.-N. Tsai, Thermal parameters optimization of a reflow soldering profile in printed circuit board assembly: A comparative study, Applied Soft Computing 12 (2012) 2601-2613.

[18] H.-Z. Han, B.-X. Li, B.-Y. Yu, Y.-R. He, F.-C. Li, Numerical study of flow and heat transfer characteristics in outward convex corrugated tubes, International Journal of Heat and Mass Transfer 55 (2012) 7782–7802.

[19] D.C. Wilcox, Turbulence Modeling for CFD, second ed., DCW Industries, Anaheim, USA, 1998. pp. 174.

[20] C.E. Zambra, N.O. Moraga, C. Rosales, E. Lictevout, Unsteady 3D heat and mass transfer diffusion coupled with turbulent, forced convection for compost piles with chemical and biological reactions, International Journal of Heat and Mass Transfer 55 (2012) 6695–6704.

[21] B.E. Launder, D.B. Spalding, Lectures in Mathematical Models of Turbulence, Academic Press, London, England, 1972.

[22] F. Mathey, Numerical up-scaling approach for the simulation of heat-transfer in randomly packed beds, International Journal of Heat and Mass Transfer 61 (2013) 451–463.

[23] B. Illés, G. Harsányi, 3D Thermal Model to Investigate Component Displacement Phenomenon during Reflow Soldering, Microelectronics Reliability 48 (2008) 1062-1068.

List of Figures: